EUROFUSION WP15ER-PR(15) 14522

L Lu et al.

Ion Cyclotron wave coupling in the magnetized plasma edge of tokamaks: impact of a finite, inhomogeneous density inside the antenna box

Preprint of Paper to be submitted for publication in
Plasma Physics and Controlled Fusion

This work has been carried out within the framework of the EUROfusion Consortium and has received funding from the Euratom research and training programme 2014-2018 under grant agreement No 633053. The views and opinions expressed herein do not necessarily reflect those of the European Commission.

This document is intended for publication in the open literature. It is made available on the clear understanding that it may not be further circulated and extracts or references may not be published prior to publication of the original when applicable, or without the consent of the Publications Officer, EUROfusion Programme Management Unit, Culham Science Centre, Abingdon, Oxon, OX14 3DB, UK or e-mail Publications.Officer@euro-fusion.org

Enquiries about Copyright and reproduction should be addressed to the Publications Officer, EUROfusion Programme Management Unit, Culham Science Centre, Abingdon, Oxon, OX14 3DB, UK or e-mail Publications.Officer@euro-fusion.org

The contents of this preprint and all other EUROfusion Preprints, Reports and Conference Papers are available to view online free at http://www.euro-fusionscipub.org. This site has full search facilities and e-mail alert options. In the JET specific papers the diagrams contained within the PDFs on this site are hyperlinked

Ion Cyclotron wave coupling in the magnetized plasma edge of tokamaks: impact of a finite, inhomogeneous density inside the antenna box

L. Lu[1,2,3,a)], K. Crombé[3,4], D. Van Eester[4], L. Colas[1], J. Jacquot[5], S. Heuraux[2]

[1]*CEA, IRFM, F-13108 Saint-Paul-Lez-Durance, France*
[2]*Institut Jean Lamour, UMR 7198, CNRS-University of Lorraine, BP70239, F-54506 Vandoeuvre Cedex, France*
[3]*Department of Applied Physics, Gent University, Belgium*
[4]*EURATOM-Belgian State, LPP-ERM-KMS, TEC partner, Brussels, Belgium*
[5]*Max-Planck-Institut für Plasmaphysik, EURATOM-Assoziation, Garching, Germany*

[a)]Corresponding author: ling-feng.lu@cea.fr

Abstract. Most present Ion Cyclotron Resonant Frequency (ICRF) heating codes and antenna codes assume the antenna sitting in a vacuum region and consider the fast wave only, which implicitly performs an abrupt density transition from vacuum to above lower hybrid (LH) resonance. The impact of the appearance of the LH resonance is entirely overlooked in their simulations. We studied the impact of densities that decay continuously inside the antenna box on near field patterns and power coupling. A new full wave code based on the COMSOL Finite Element Solver has been developed to investigate this topic. It is shown that: up to the memory limits of the adopted workstation, the local RF field pattern in low-density regions below the LH resonance changes with the grid size. Interestingly and importantly, however, the total coupled toroidal spectrum is almost independent on the mesh size and is weakly affected by the presence of the density profile inside the antenna box in dipole toroidal strap phasing. This suggests one can drop out this density for coupling studies to speed up the computation. Simulation also shows that varying the density gradient in the fast wave evanescence region has no significant effect on wave coupling.

I. INTRODUCTION

Ion cyclotron resonant heating is used as the main heating method in the current-state magnetic fusion devices. These waves oscillate in time as exp(iw_0t) at a frequency $w_0/2\pi$ around 25-100MHz, and are excited by phased arrays of radiating current straps [1, 2]. Provided the cold plasma approximation is justified, one can describe the plasma by the cold plasma dielectric tensor [3]

$$\boldsymbol{\varepsilon} = \begin{pmatrix} S & iD & 0 \\ -iD & S & 0 \\ 0 & 0 & P \end{pmatrix} \begin{matrix} \perp 1 \\ \perp 2 \\ // \end{matrix} \quad (1)$$

where S, D and P can be found in [3]. Their values vary with plasma density. The signs //, $\perp 1$ and $\perp 2$ indicate the parallel and two perpendicular directions w.r.t the magnetic field. Note the signs of the off-diagonal terms changed due to the engineering convention we use. Within the cold plasma regime, there is a plane wave description for two type of waves that could be exist under the frequency range mentioned previously. The orientation of the straps with respect to the confinement magnetic field is chosen so that it mainly excites the fast wave, which has a large electric

field in the poloidal direction of a toroidal device. Another mode with vastly different polarization, the slow wave, can also be excited parasitically by the fast wave antenna. The parallel electric component of the slow wave is essential in the RF sheath formation [4]. Some important features about these two waves are revealed by the decoupled dispersion relations, which read,

$$(slow\ wave)\ n_{\perp S}^2 = P(1-\frac{n_{//}^2}{S}) \quad (2)$$

$$(Fast\ wave)\ n_{\perp F}^2 = \frac{(R-n_{//}^2)(L-n_{//}^2)}{(S-n_{//}^2)} \quad (3)$$

$n_{//}$ and $n_{\perp}$ are the parallel and perpendicular refractive indices, respectively. *R* and *L* are linked by the Stix tensor components, by *R=S+D*, *L=S-D*. A plot of above dispersion relations for typical range of tokamak densities is shown in **Figure 1**.

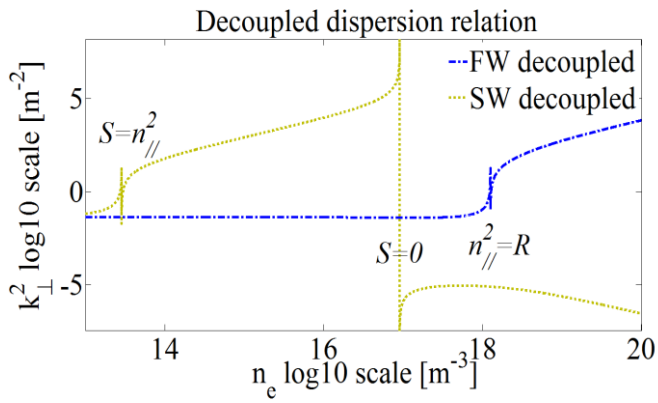

Figure 1. Square of the wave vector component normal to B_0 from the dispersion relation of the decoupled slow wave and fast wave V.s. density. Following parameters are used, frequency 48MHz, magnetic field B_0=2.32T at $n_e=10^{18}m^{-3}$, parallel wave number $k_{//}$=5 m^{-1}, D plasma

One can see the fast waves can propagate into high density plasma, which is why this type of wave is often used as heating wave [2], whereas the slow wave only propagates in plasmas with fairly low densities**.** Most current-day ICRF heating codes and antenna codes [5, 6, 7] assume the density close to the antenna is sufficiently low to allow it being neglected altogether, and restrict themselves to the fast wave excitation. In reality, a low but finite density is actually present inside the antenna box and a fast wave antenna parasitically excites the slow wave. So an intriguing question is whether this presence of density profile inside antenna will significantly change the results outside the antenna box. Furthermore, since no accurate density measurement presently exists experimentally inside the antenna box, one may ask whether an accurate density profile is essential? The power carried by the fast wave is the main heating power. An important characteristic parameter in the fast wave power coupling studies is the fast wave R-cut off layer. It is derived by setting $R = n_{//}^2$ in the fast wave dispersion relation Eq.(3). For a given $n_{//}$, the fast wave is evanescent below this layer and propagating above. The length between antenna straps and the R cut-off layer is known as the fast wave evanescence length. The power coupling roughly decays exponentially w.r.t the fast wave evanescence length [8,9,10,11]. For tokamak parameters like those of Tore Supra used on **Figure 1**, the R-cut off layer for the main $n_{//}$ of a Tore Supra antenna with antisymmetric (dipole) strap phasing locates at the plasma density close to 10^{18} m^{-3}. For smaller $n_{//}$, the R-cut off layer shifts from the center plasma towards the wall. So another question is how much the density profile inside antenna box can affect R-cut off layer and the coupling power.

The physical behavior becomes more complicated when a special layer called Lower Hybrid (LH) resonance [12] appears inside the antenna box. The place where the slow wave has its LH resonance is defined by *S*=0, where *S* is the perpendicular diagonal component of Stix tensor. For typical tokamak parameters, i.e. ToreSupra, the LH resonance appears at the plasma density approaching 10^{17} m^{-3}. The density is well beyond the LH resonance at the last closed flux surface but well below it or marginally below it at the position of the straps. Hence the LH resonance is a natural ingredient of wave behavior close to launching structures. Numerous literatures have talked about this resonance. Puri

discovered the collisional energy absorption at the LH resonance leads to a high plasma heating efficiency [13]. Bellan showed that around this resonance, the dispersion relations Eq. (2)-(3) need to be replaced by the fully coupled dispersion relations and mode conversion can occur [12]. Crombé and Van Eester discussed the wave behavior below the LH resonance [14], where the slow wave starts to propagate. One can see from the slow wave dispersion relation, Eq.(2), that in a region where *P* is real negative and *S* stays between 0 and $n_{//}^2$, wave with high $n_{//}$ has larger $n_{\perp S}^2$ and thus more likely to propagate. As a consequence, slow wave having a nature of short wavelength can be very sensitive to the mesh size in the numerical simulations. An unusual situation is met at the LH resonance where the wavelength of the slow wave shrinks to zero. One may wonder if it is possible to numerically capture this wave sufficiently accurate. And if it is not as claimed in [14], does a non-converged result inside antenna box significantly affect the results outside the box? It is interesting to know if this thin layer has a global impact or not. Another question being whether the power carried by the slow wave to this resonance is significant or not.

A 2D full wave coupling code with tilted magnetic configuration [15, 16] dedicated to study wave coupling problems in a collisionless magnetized cold edge plasma has been developed and tested based on COMSOL Multiphysics finite element solver [17]. The details of this code are shown in the next section. In this paper, it has been used to investigate the radiated electric fields in the presence of a finite, inhomogeneous density inside the antenna box. Essentially, the fields below lower hybrid resonance, and the power coupling property with the appearance of lower hybrid resonance were examined in detail and the results of this study will be discussed here.

The structure of this paper is the following: Section II gives the specifications of the code and the parametric setup for the numerical tests, i.e. density profiles, mesh size, magnetic field tilt angle and phasing. Section III and IV analyze the simulated RF near fields pattern inside the antenna box. Section V shows the radiated power at the antenna aperture and the role of the density gradient in front of antenna straps on the fast wave power coupling. Section VI is the final discussion and conclusion.

II. 2D FULL WAVE COUPLING CODE WITH TILTED B_0 AND SIMULATION PROGRAM

To answer the questions being asked in the introduction, we need a dedicated numerical code. It should cover the following physics, a) Fields are excited by a realistic ICRF antenna model includes all the essential elements, antenna box, strap, limiter et al. b) Fields need to be solved in a tokamak (cold) plasma, which is described by a full dielectric tensor. c) Both the fast wave and the slow wave should be considered simultaneous. d) It should accommodate a continuous and inhomogeneous plasma density across R-cut off layer and LH resonance. e) Fine mesh is needed in order to capture the short wavelength structure. f) As any other numerical code, it should save the computational resource as much as possible. g) At last, for our specific interests, implementing RF sheaths should be easy in a later stage of development.

There are plenty of numerical codes dealing with the wave propagation and coupling. Some codes [6] have a simplified geometry but rely on the input from other codes with more complex geometry. The off-diagonal term in the plasma dielectric tensor introduces the coupling between the fast wave and the slow wave. However most of the code based on CST microwave studio [18] and HFSS software [1] do not treat the typical gyrotropic properties of a magnetized plasma. Some codes need to discretize the plasma into a series of slabs [19], in order to impose a plasma density. Some advanced codes based on method of moment have difficulties to include density inside antenna box [5] and they assume the fast wave is the only propagating wave. Codes written in FORTRAN [20] are constrained by the limits of the mesh density and the choice of finite element shape.

Our 2D full wave coupling code has a realistic 2D geometry, which takes advantage of the finite element solver in COMSOL, shown in **Figure 2,** where the x direction corresponds to the toroidal direction, y is the radial direction and z (out of plane component) is the poloidal direction in a Tokamak geometry where the curvature effect has been ignored. It is a cut from the middle plane of the 3D realistic ICRH antenna. The antenna includes two straps, the antenna box, central septum and lateral limiters, indicated as the blank components. All passive metallic elements are treated as Perfect Electric Conductor (PEC): at their interface with the plasma the tangential RF electric field vanishes. The antenna aperture is shown as a dashed line. COMSOL uses engineering convention as noted before. This convention will be used in the following sections.

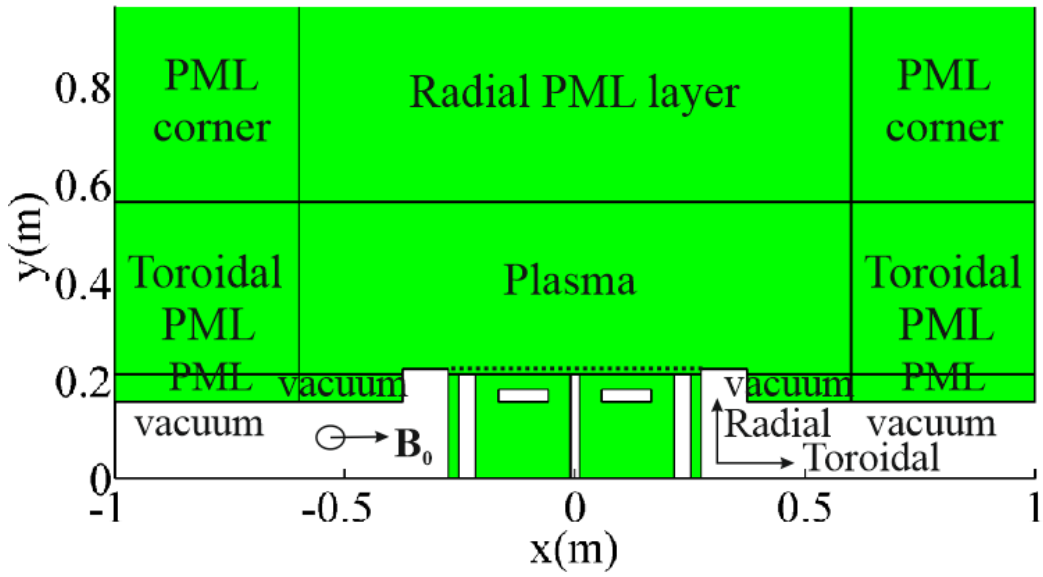

Figure 2. Schematic view of 2D full wave coupling code with tilted B_0. Dashed line is the antenna aperture

The cold plasma is described by the Stix dielectric tensor (expressed in COMSOL coordinates), which is rotated under the following convention,

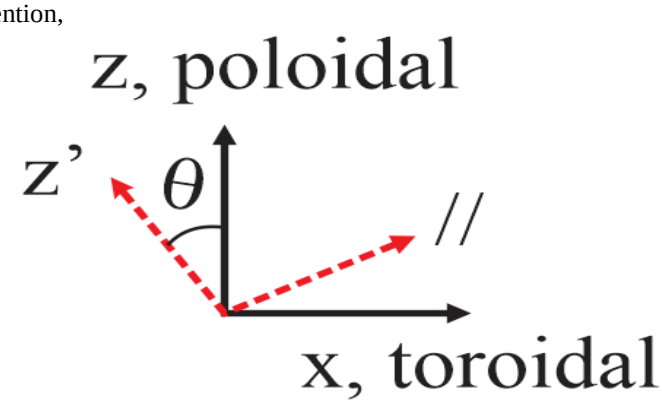

Figure 3. Geometry (x, z) and magnetic field (//, z') based frame

The code plasma tensor expressed in the COMSOL geometry reads,

$$\varepsilon' = \begin{pmatrix} S\sin^2\theta + P\cos^2\theta & iD\sin\theta & -S\sin\theta\cos\theta + P\sin\theta\cos\theta \\ -iD\sin\theta & S & iD\cos\theta \\ -S\sin\theta\cos\theta + P\sin\theta\cos\theta & -iD\cos\theta & S\cos^2\theta + P\sin^2\theta \end{pmatrix} \begin{matrix} x-toroidal \\ y-radial \\ z-poloidal \end{matrix} \quad (4)$$

where the tilt angle θ is the angle between magnetic field line and toroidal direction in toroidal-poloidal plane. It turns out that by adding this tilt angle, which did not appear in the previous version of this code, can introduce the fast wave in describing Direct Current (DC) sheath biasing by RF sheaths rectification [21]. Thus make it compatible with another sheath code which is under development now in Cadarache [21]. Physically oblique magnetic field also provides a sort of 'mode conversion' that an incident slow wave needs to generate a reflected fast wave in order to fulfill the PEC boundary conditions at the wall [22]. To save the computational resource, our simulation domain is radially and toroidally close to the vicinity of a wave launcher. We assume the wave transmitted to the central plasma never comes back to the antenna (single-pass absorption), which could occur in a real hot tokamak plasma. Under this assumption, the Perfect Matched Layer (PML) is used in the code surrounding the plasma region, to emulate radiating

boundary conditions in two directions. The propagating fast wave is damped artificially in these layers. The PML technique described in [15] is extended to tilted $\mathbf{B_0}$ [16] and has been recently further adapted to a curved cylindrical geometry [23]. In this 2D code, the poloidal geometry is assumed to be infinite and homogenous. As a consequence, the poloidal derivative is set to zero. A 3D simulation tool is developed in parallel with this work by one of the co-authors [23]. It is however extremely memory demanding, and the convergence of the iterative solver is much more difficult to achieve. Thus all the simulations in this paper are done using the 2D code.

In this paper we use a plasma solely composed of D ions. Furthermore, the following Tore Supra like parameters are taken [15]: magnetic field at aperture $\mathbf{B_0}$(y=0.224)=2.32T, RF wave frequency 48MHz. The magnetic field strength scales as $1/R_a$, with R_a the major radius axis. In our adopted geometry, R_a=3.382-y. All the simulations in this report are done using a dedicated workstation with 64Gb of RAM memory.

A set of continuous density profiles is used inside the antenna box, the details are shown in **Table 1**. **Figure 4** is the density profile from Tore Supra shot TS 40574 and it is used outside of the antenna box. **Figure 5** is the density profiles inside the antenna box, corresponding to the density profiles listed in **Table 1**.The LH resonance appears under density 3 and 4.

Density	Value inside antenna box (m^{-3})	Density at wall (m^{-3})	Location of LH resonance
0	0	0	Not present
1	Extrapolate experiment profile to 10^{17}	1×10^{17}	Not present
2	$n_e=10^{18}\exp(-(0.2195-y)/0.0933)$	9.5×10^{16}	Not present
3	$n_e=10^{18}\exp(-(0.2195-y)/0.0477)$	1×10^{16}	y=0.1056m
4	$n_e=10^{18}\exp(-(0.2195-y)/0.0318)$	1×10^{15}	y=0.1434m

Table 1. Density profiles used inside the antenna box

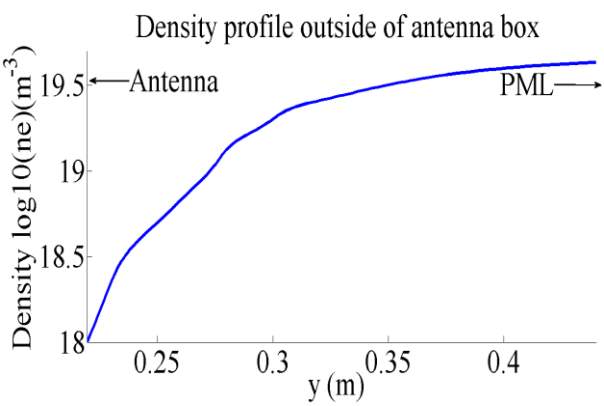

Figure 4. Density profiles above the antenna

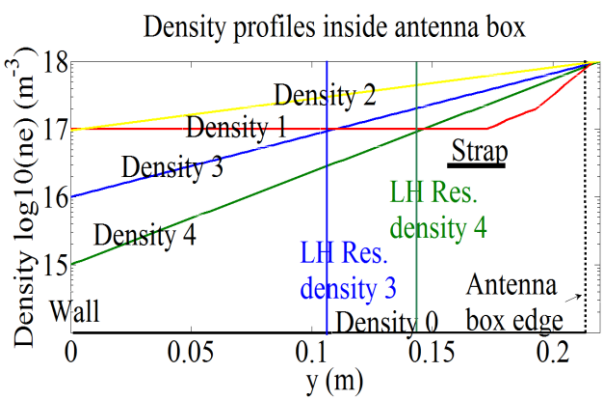

Figure 5. Density profiles inside the antenna box. Vertical solid lines indicate the locations of the LH resonance. Vertical dot line specifies the edge of the antenna box.

Our major goal is to investigate the field structure inside the antenna box, where the slow wave may become propagating. As mentioned above the slow wave generally has a short wavelength. This requires a very fine mesh. In the following simulations, we use four different meshes with triangular shape through all the domain.

	Mesh 1	Mesh 2	Mesh 3	Mesh 4
Grids size (x, y)	4mm*4mm	4mm*2mm	2mm*4mm	2mm*2mm
Number of grids in each individual box	52*54	52*108	104*54	104*108
Specific refinement	Up to 800*800			

Table 2. List of meshes used in the simulations

In those regions where the slow wave is supposed to be present, i.e. near the antenna aperture, a mesh refinement is added, generally 4 times or 8 times finer than the other regions. A typical simulations time using the above mesh is around 6 minutes. In case we need to check the convergence with extremely fine mesh, more intensive meshes are

used, up to 800*800 grid points in each individual box. These extremely requirement in terms of memory explain why we restrict our investigation to two dimensions.

The magnetic field in this code can be tilted continuous from -90° to 90°. We start from non-tilted (0°) case, then pick up a realistic angle (for Tore Supra) 7° and a large angle 60° for all the field analysis. In the power coupling analysis, a scan of tilt angle from -90° to 90° is conducted for the sake of completeness although extreme tilts are clearly unrealistic in tokamaks.

The waves are excited by imposing current on the straps. All the simulations are done with 1A poloidal current imposed on each strap. Both antiparallel strap currents (dipole phasing [0 π]) and parallel ones (monopole phasing [0 0]) are considered in order to change the radiating toroidal spectrum.

III. NEAR FIELD PATTERN ABOVE THE LOWER HYBRID RESONANCE

This section investigates the RF electric field pattern in the region above the lower hybrid resonance. From the dispersion plot, **Figure 1**, we know only the fast wave is propagating in this region. Fast wave has a large poloidal electric field, thus it is reasonable to look at this electric component. **Figure 6** takes density profile 3 in the antenna box. The electric field is anti-symmetric as the magnetic field is non-tilted. One can see the fast wave is propagating in the plasma and being damped inside the PML. The perpendicular wavelength of the fast wave is around 15cm, which is compatible with the calculation from the dispersion relation, Eq. (3) using a parallel refractive index $n_{//}$=9.14. The poloidal electric field changes less than 1% when switching from density 0 (vaccum) to density 3 and it varies less than 0.1% between density 3 and density 4 (**Figure 7**). **Figure 8** shows the differential poloidal electric field taken from two simulations with different mesh grids, while other parameters are the taken the same as **Figure 6**. The scale of differential field reduces an order of 3, compared to **Figure 6** . **Figure 9** is a zoom in of the region around straps surrounded by a red rectangle in **Figure 8**. It shows the relative difference of poloidal electric field is less than 10^{-3}. The relative difference is twice larger under large tilt angle, i.e. theta=60°. One may expect in this case the antenna excites a larger part of slow wave rather than fast wave. So it will be more sensitive to the mesh.

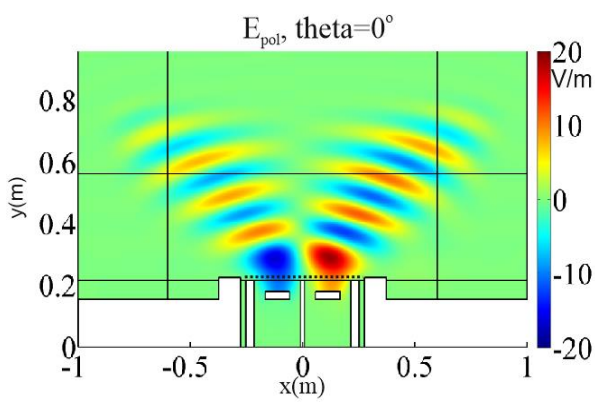

Figure 6. Real part of the poloidal electric field, theta=0°, mesh 2, density 3, dipole phasing

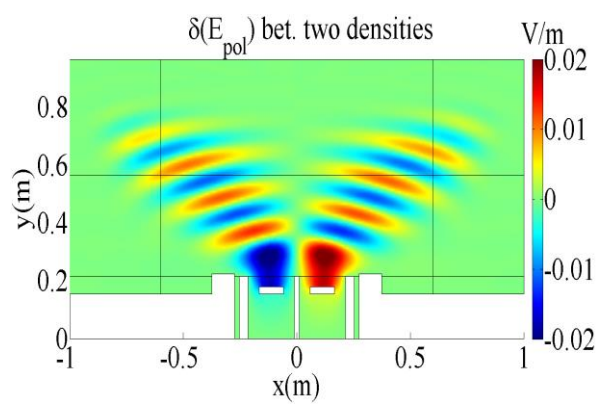

Figure 7. Differential field map for the real part of the poloidal electric field between density 3 and density 4

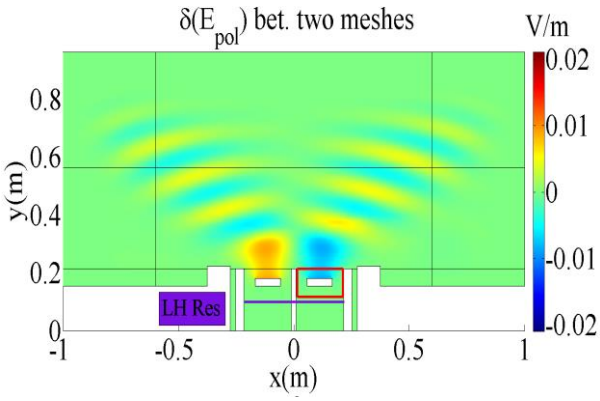

Figure 8. Differential field for the real part of poloidal electric field, between mesh 2 and mesh 1. Horizontal line: location of LH resonance. Rectangle: box region shown on **Figure 9**

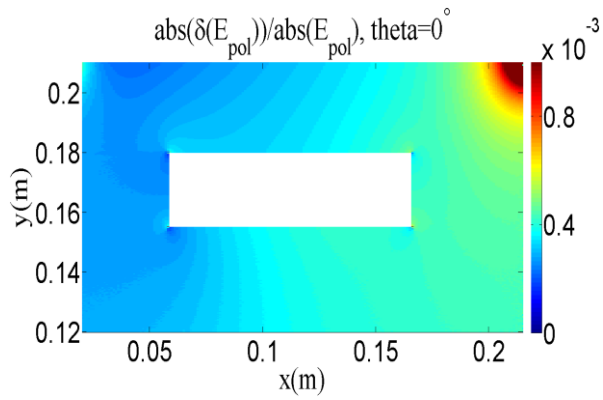

Figure 9. Relative error of poloidal electric field. Zoom in the antenna strap's region surrounded by rectangle in **Figure 8**

The radial electric field is also independent on the mesh outside of the antenna box. While inside the antenna box, compared to vacuum case, new filaments along toroidal direction appear in both toroidal electric field and radial electric field, see **Figure 10**-**Figure 11**. Smoothing the corner, imposing different distributions of surface current, i.e. hyperbolic cosine, do not totally remove these filaments.

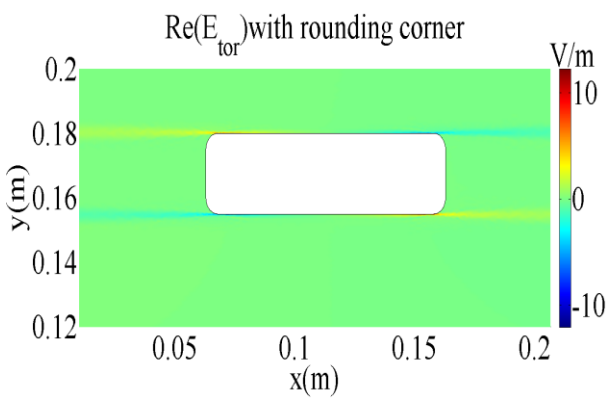

Figure 10. Toroidal electric field in the antenna strap region surrounded by rectangle in **Figure 8**, with hyperbolic cosine distribution of RF current over straps with rounded corners

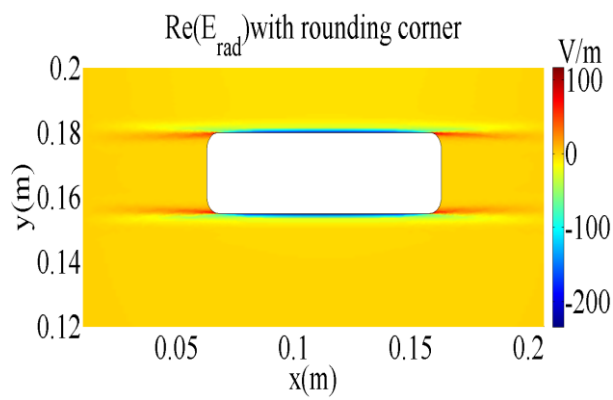

Figure 11. Same as **Figure 10**, radial electric field

From **Figure 9**, we see the poloidal electric field is determined by the imposed current and is thus independent of mesh. However unlike in a vacuum antenna, where electric fields on the strap surface normally have a converged solution, further tests showing in a plasma-filled antenna box, it is more difficult to ensure numerical convergence of the toroidal and radial electric field around the strap. A simulation with extremely intensive mesh showing the field at the corner points is still not converged, see **Figure 12**. This non-converged problem appeared in the neighborhood region of antenna in the presence of plasma [24] is most likely caused by the excitation of the slow wave. A check of polarization also gives the same indication, that a slow wave fulfills the magnitudes of all the electric components around the strap. Besides, the polarization of the slow wave indicates that the radial electric component of the slow wave is coupled with its parallel electric component [25]. The latter is increasing with the tilt angle. Thus one can anticipate that the radial electric field also increases with the tilt angle. Simulation shows that the real part of the radial electric at theta=20º is indeed twice larger than idem value at theta=0º.

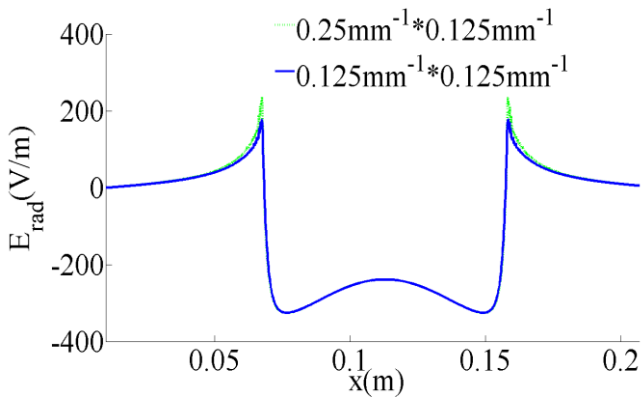

Figure 12. Toroidal distribution of Re(Erad) on the front face of the right strap, under two very dense symmetric meshes, other conditions are the same with **Figure 11**

COMSOL is unable to go to further beyond the mesh used in **Figure 12**, due to the memory limits. Thus a semi-analytical model has been built to further investigate the physics related to the filament. The details can be found in the Appendix. For simplicity, the field is excited by a sheet of poloidal current in this model. It has a 2D geometry with 3 metallic walls and 1 radiating boundary. By assuming the fast wave and the slow wave are decoupled, one can separate the contribution form the fast wave and the slow wave to the total electric field. This model has successfully reproduced the filament surrounding the current sheet by conducting Fourier analysis for a sufficient large number of plane wave eigenmodes. The spatial resolution is 10 times' finer than **Figure 12**. Results show that this filament persists under such a high resolution and it is indeed associated with the slow wave, which states that a fast wave antenna can excite the slow wave. The slow wave is strongly evanescent here and is sensitive to stix tensor element *P*. One can estimate that the perpendicular evanescence length is changing with the square root of P, Eq. (5). This was confirmed by manually changing the *P* value, see the Appendix

$$l_{\perp S} \approx \frac{2\pi}{k_0 n_{\perp S}} \approx \frac{2\pi}{k_0\sqrt{|P|}} \quad (5)$$

.

In reality, most of the excitation is done through imposing a certain voltage on the straps, thus the currents on the strap are computed self consistently. Unlike we fix the direction of current flow on the antenna here, in a voltage excitation, the tilt angle is relevant w.r.t. the direction in which the current flows on the antenna. Self-consistent computations give rise to image currents on metallic objects and that these locally play the role of 'antenna' as well. These may change the slow wave excitation. Besides, a slow wave can also be generated via mode conversion when the geometry has a shape transition [26]. A voltage excitation and curved geometry has been implemented in the 3D version of this wave coupling code [23].

IV. NON CONVERGED FIELD BELOW THE LOWER HYBRID RESONANCE

In his section, the fields near and below the lower hybrid resonance are shown. We use the density 3 and density 4, in which the LH resonance is crossed inside the antenna box. As said before, only the slow wave is propagating in this region. Near lower hybrid resonance, slow wave has a characteristic of electrostatic wave. In non-tilted magnetic case, its polarization reads [27],

$$\frac{E_{rad}}{E_{tor}} \approx \frac{n_{\perp S}}{n_{//}} \approx \pm\sqrt{-P/S} \quad (6)$$

Hence one can know the propagation direction from the ratio of relevant electric fields. **Figures 13** (a)-(b) use exponential density profile 3 and 4 with the same mesh 2. Locations of the lower hybrid resonance are indicated by

red dot line, specifically at y=0.1056m and y=0.1434m. One can see below the resonance, new fields start to grow and as the density decreases, more and more modes appear. In dipole phasing, this structure is anti-symmetric between two individual boxes, with respect to antenna septum, under the condition of symmetrical mesh. The radial electric field is about 20 times larger than the toroidal electric field, which is consistent with the typical ratio of $\sqrt{-P/S} \approx \sqrt{500/1} \approx 20$, so the slow wave mainly propagates along the radial direction. The poloidal electric field is still independent on the mesh in this region.

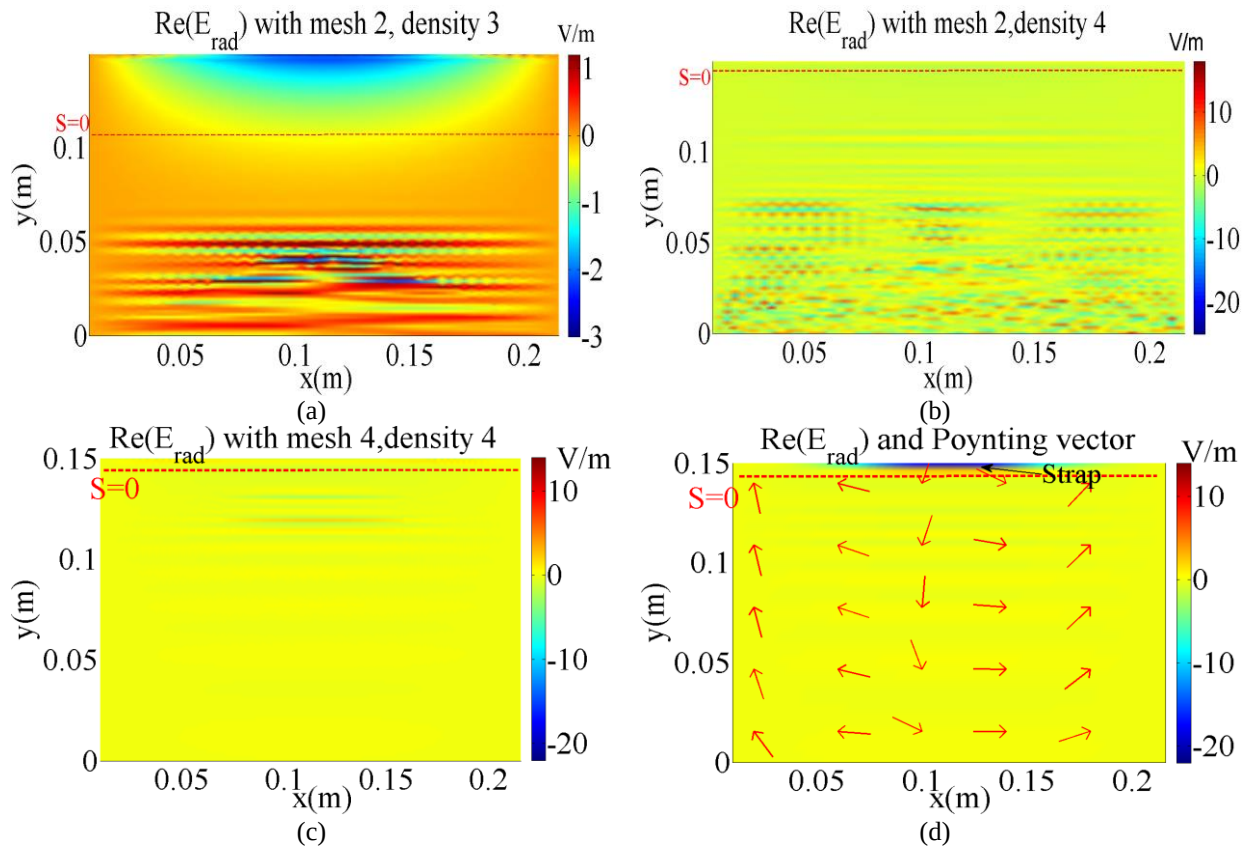

Figures 13. (a)-(b). Real part of the radial electric field with different density profiles, but the same mesh. Dipole phasing, theta=0^0. (c). the same simulation as (b) but with mesh 4. (d) Radial electric field, using density 4, the same mesh size as mesh 4 but with square grid, instead of triangle. Red arrows indicate the normalized real part of the Poynting vector

Slow wave propagates between the lower hybrid resonance ($S = 0$) and $S = n_{//}^2$. One generally considers the parallel refractive index $n_{//}$ is determined by the antenna geometry and phasing in the main plasma, which can approximately be seen as an invariant spectrum. But this may be not the case in the region below LH resonance. From **Figures 13** (b), one can see the slow wave behaves like cavity modes, where modes with $k_{//} = \frac{2\pi n}{L}$ (with n an arbitrary integer and L the toroidal dimension of metallic box) are selected and added up together. Aside from propagating along radial direction, it bounces between two toroidal metallic walls. The toroidal modulation of the small-scale structure appeared in the lower part of **Figures 13** (b) agrees with the grid's size.

From the slow wave dispersion relation, Eq. (2), one knows that in its propagating region, for a given $k_{//}$, the perpendicular wave vector $k_\perp$ decreases as the density decreases, see the yellow line in **Figure 1**. This is consistent with **Figures 13** (a), where the $\lambda_\perp$ (perpendicular wave length) is increasing as the density decreases from upper to bottom.

Compare **Figures 13** (b) with (a), we see when the density switches from density 3 to density 4, more modes with lower $k_{//}$, thus larger $\lambda_{//}$ (parallel wave length) mode become propagating. This can be understood from $k_\perp^2 = k^2 - k_{//}^2$, when the density decreases, k^2 are decreasing, so in order to have a positive $k_\perp^2$, one needs a smaller $k_{//}$. Although

the propagative region for the slow wave mode is surrounded by 3 metallic walls and one resonance, it is not a lossless resonant cavity for the slow wave. The energy of the slow wave can be transferred through mode conversion to the fast wave at the wall (under tilted magnetic field) or at the LH resonance. Since no damping mechanism is considered in the box, i.e. frequency and all dielectric tensor element have a real value, all the radiative energy (real part of power flow) should finally be transferred to the fast wave, which then carries this power out of the antenna box. This is shown in **Figures 13** (d) where the direction of the normalized real Poynting vector indicating the power flow indeed goes to the LH resonance and lateral metallic walls. Only the slosh power (imaginary part of power flow) then remains bouncing inside box.

Given the small radial scales appearing in **Figures 13**, one can anticipate that the mesh size near the wall might affect the numerical results. To see this, we check the case where we add a specific mesh refinement in the region within a distance of 0.008m to the antenna box wall. We find that **Figures 13** (a) with density 3 changes 10% of values, while **Figures 13** (b) with lower density (density 4) changes 200%.

A further test shows that the non-convergence persists up to the memory limits of the adopted workstation (800*800 grid points inside each individual box). This confirms the observation from another finite difference code [14] about the non-convergence behavior of the field below lower hybrid resonance. This instability is increasing under larger tilt angle which is again coincides with the fact that antenna excites more slow wave in that case. No explicit dependence on antenna phasing is observed. This is not surprising for the simulations considered. The straps are housed in individual boxes. The LH resonance is rather deep inside the box. Each slow wave resonant cavity may be therefore mainly influenced by one single strap.

V. POWER COUPLING AND RADIATING SPECTRA

The radiated power is the key quantity in the wave coupling studies. In this 2D code, the power emanating from the strap is denoted as

$$-\frac{1}{2}\mathrm{Re}(\int_V \mathbf{E}\cdot\mathbf{J}^* dV) = \mathrm{Re}(\mathbf{P}) \quad (7)$$

where the Right-Hand Side (RHS) means the real part of $\mathbf{P} = \frac{1}{2}\oint_S (\mathbf{E}\times\mathbf{H}^*)\cdot\mathbf{n}dS_a$ i.e. the power flow through a closed surface S_a surrounding the strap. **J** is the imposed surface current on the strap. The Left-Hand side (LHS) is a volume integral to the antenna region. Since we only imposed the poloidal current, the LHS can be reduced to a line integral to a scalar product. Since our radiation medium is loss-less, we checked that the power flow at the antenna aperture exactly equals to the line integration at the strap. From **Figure 8**, we know that the poloidal electric field is almost independent on the mesh and the current is imposed externally. So the total emanating power as well as the power flow in the plasma is independent on the mesh.

Most antenna design codes assume the antenna is sitting in a vacuum region. It is interesting and important to check how different the power and the electric field near antenna aperture are when one compares the difference between a plasma-filled and a vacuum antenna box. In the following test, we measure power by doing a line integral of radial power flow, the real part of Poynting vector, across the antenna aperture (dashed line in **Figure 2**).

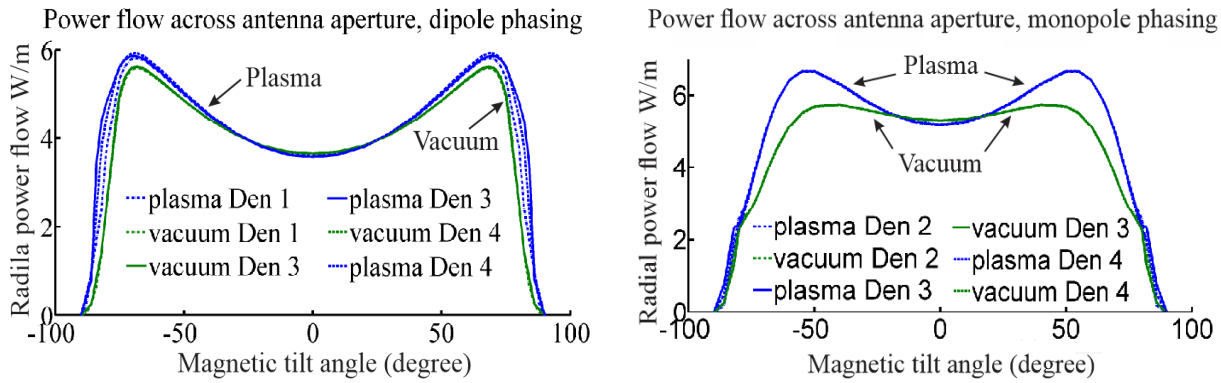

(a) (b)

Figures 14 . Radial power flow across the antenna aperture versus magnetic field tilt angle, (a) dipole phasing with density profiles 1, 3 and 4. (b) monopole phasing with density profiles 2, 3 and 4. Blue curves indicating plasma-filled antenna box. Green curves show simulations with vacuum in the antenna box.

Figures 14 shows the variation in the radiated power for 1A on the straps, over a scan of tilt angle. Mesh 2 is used. In the simulations with a vacuum antenna box, the density profiles are cut at the antenna box edge, dot line of **Figure 5**. In **Figures 14,** the power level in monopole phasing is higher than in dipole phasing. This is not surprising since the evanescence region for the fast wave is shorter in monopole phasing than in dipole, thus less power is reflected to the straps. For dipole phasing, power seems independent of whether antenna is in plasma or in vacuum. For monopole phasing, there is up to 20% difference between the power launched from an antenna immersed in a plasma compared to one sitting in vacuum when scanning over all possible tilt angles. In both cases, power coupling is not sensitive to the density profile shape. In order to check this difference, we plot the toroidal power spectrum obtained by conducting Fourier transform near the antenna aperture at theta=60° where the difference gets largest. We see clearly from the power spectrum, (**Figure 15**) that under monopole phasing the power gap between plasma filled-in antenna and vacuum antenna is larger than that in dipole phasing. The farthest lobe we can see in **Figure 15** is located at the toroidal refractive index n_x=-35, corresponding to a wavelength of 0.006m. As a comparison, our grid size is 2.5×10^{-4}m, so all the spectrum lobes have already been well captured in obtaining the results of **Figures 14**.

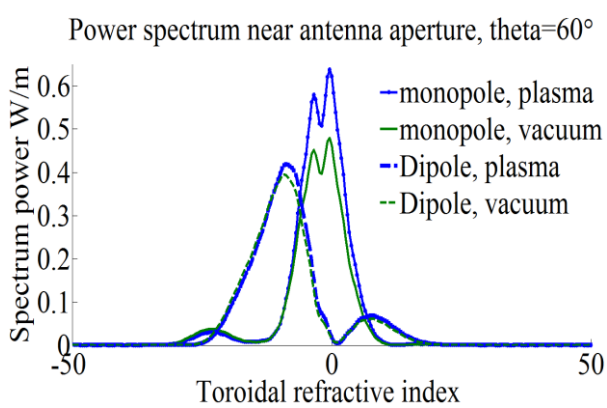

Figure 15. Power spectrum at large tilt angle theta=60°, plasma density 3 is used for blue curves

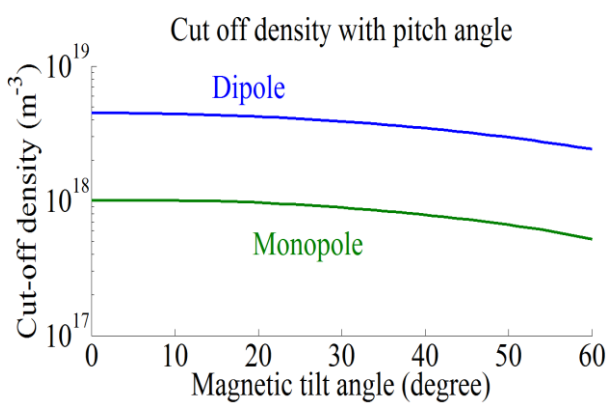

Figure 16. Fast wave cut-off density, Dipole phasing n_x=9.14, monopole phasing n_x=4.5 are used

The drop of power spectrum at low n_x in monopole phasing can be understood by looking at the fast wave cut-off layer, as introduced in the first part. Starting form Eq. (3), when coordinates rotate in the toroidal-poloidal plane, the parallel and perpendicular refractive index can be expressed as

$$n_{\perp F}^2 = n_{z'}^2 + n_{y'}^2 = n_y^2 + (n_z cos\theta - n_x sin\theta)^2$$
$$n_{//}^2 = (n_x cos\theta + n_z sin\theta)^2 \quad (8)$$

Inserting the above two equations into the dispersion relation, and noting that in our 2D geometry, n_z=0. Finally we have

$$n_y^2 + n_x^2 sin^2\theta = \frac{(n_x^2 cos^2\theta - R)(n_x^2 cos^2\theta - L)}{S - n_x^2 cos^2\theta} \quad (9)$$

The R cut-off layer by definition corresponds to n_y=0, thus we obtain,

$$n_x^2 sin^2\theta = \frac{(n_x^2 cos^2\theta - R)(n_x^2 cos^2\theta - L)}{S - n_x^2 cos^2\theta} \quad (10)$$

Figure 16 plots the fast wave cut off density versus the magnetic tilt angle for two toroidal wavenumbers n_x, characteristic of each phasing. As a reference, the density around antenna aperture is about 9×10^{17} m^{-3}. In dipole phasing, due to the large n_x, the cut-off layer is well above antenna box, thus the fast wave is evanescent inside the antenna box, no matter the box is in vacuum or filled by plasma. However, in monopole phasing, the cut-off layer is generally inside antenna box under large tilt angles, thus the fast wave evanescence region is larger in a vacuum antenna than in an antenna filled with plasma. With the increasing of tilt angle, the cut off layer from Eq. (10) is shifting to the edge, in other words the cut off density is decreasing. This explains the power in **Figures 14** is increasing as the evanescent length is decreasing with tilt angle increasing. Then under large tilt angle it drops down dramatically as the fast wave antenna changes to a slow wave antenna.

Dipole phasing is used as the main heating phasing in the present ICRH experiments for its better power absorption by the plasma. For this phasing, the effect of density gradient in the fast wave evanescence region on power coupling is also studied. We tested three tilt angles, i.e. theta=0^0,7^0 and 20^0. For each tilt angle, we calculated the R cut-off density using Eq. (10) and its radial location in our reference profile. Then starting from the R cut-off, a set of exponential density profiles with different decay lengths was imposed, as shown in **Figure 17**. The density is assumed to have the following form,

$$n_e(y) = n_co * \exp((y - y_co)/L) \quad (11)$$

Where n_co, y_co are the cut off density and its location, y the radial coordinate and L the density decay length.

Results show that changing density gradient in the fast wave evanescence region can drive power variations up to 5%, see **Figure 18**.

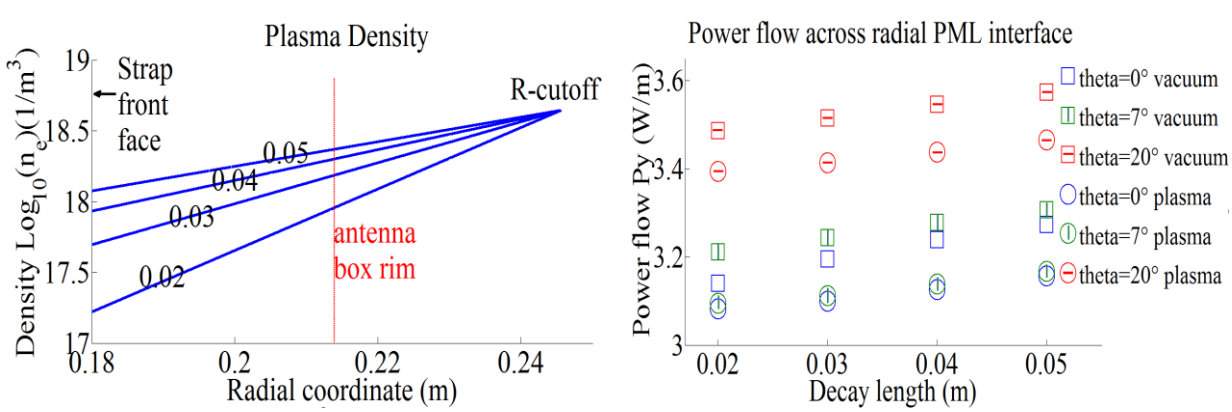

Figure 17. Test density profiles in the fast wave evanescence region, theta=0°. Labels indicate the exponential decay length *L* in m

Figure 18. Power flow across radial PML interface versus density decay length. In case of a vacuum antenna box, density is cut at antenna box rim, shown in **Figure 17**

VI. DISCUSSION AND CONCLUSION

The presence of tenuous plasma inside an ICRF antenna box can make the numerical simulation of local RF electric field more problematic when the density profile crosses the LH resonance than in the absence of this critical layer. Up to the memory limits of our dedicated workstation, radial and toroidal RF fields below the LH resonance did not converge with the decreasing mesh size. They exhibited sensitivity to small local density changes. This is probably due to the conjunction of short wavelength for the slow wave and the presence of a lossy cavity for this mode inside the antenna box. It is critical to be aware of this non-convergence when studying near field effects inside the antenna box. Another similar case is that a slow wave can also be excited in the vicinity of the straps by a fast wave antenna, however it only causes local numerical instabilities here due to its strong evanescence.

With a dominant poloidal current imposed on the straps, it was shown that the poloidal electric field and thus the total excited power is independent of the mesh even in the presence of the LH resonance behind the straps. This guarantees that the ICRF power transmitted to the main plasma *via* the fast wave is also independent of the mesh or the non-convergence property of the fields inside the antenna box. In a 3D antenna with voltage excitation, this point may need further investigations. All the radiated power carried by the slow wave is transferred to the fast wave. In a situation where the R-cutoff layer for the fast wave is well outside the box, e.g. in dipole phasing with Tore Supra profiles, the total power coupled to main plasma is indifferent with the plasma density inside the antenna box so that one can drop out the low density inside the antenna box when studying coupling issues. In monopole phasing with Tore Supra density profiles, simulations show that there is a maximum 20% of power increase due to the presence of plasma, for large tilt angles. The distinction comes from the fact that the fast wave evanescence length for low $k_{//}$ changes. Hence modeling low $k_{//}$ scheme with antenna staying in vacuum may need to be re-considered. The present model ignores parasitic damping (collisional) and sheath effects. A situation similar to the LH resonance might arise when peripheral cyclotron layers are located inside the antenna box. The poloidal gradient, which was ignored in our simulations, will likely play a key role at the study of density modifications by ponderomotive force [28]. Those effects will be left for the future study. The density measurement in the fast wave evanescence region is affected by the largest uncertainty [29] due to both measurement issues and large fluctuation levels [10]. This is again crucial in determining near field. Nevertheless, changing density gradient in the evanescence region can maximally affect power coupling up to 5%. One can thus still model the power coupling to plasma with a fairly good precision despite some uncertainties in low-density part of the profile. All simulations however stress the need to measure precisely the R-cut off radial position in order to get accurate estimation of ICRF wave coupling properties. This is a strong motivation for implementing density diagnostics as close as possible to the wave launches.

ACKNOWLEDGMENT

This work has been carried out within the framework of the EUROfusion Consortium and has received funding from the Erasmus Fusion-DC and the Euratom research and training programme 2014-2018 under grant agreement No 633053. This is a part of work conducted under work package enabling research WP15-ER-01/CEA-05. The views and opinions expressed herein do not necessarily reflect those of the European Commission.

APPENDIX: FILAMENTARY RF ELECTRIC FIELDS AROUND STRAPS IN PLASMA-FILLED BOX AS SLOW WAVE STRUCTURES EXCITED BY POLOIDAL RF CURRENTS

This appendix proposes an explanation for the filamentary structures observed in simulated 2D RF field maps around poloidal current straps radiating in plasma-filled antenna box. The qualitative phenomenology to be reproduced includes the following observations:

- 1°) "Filaments" appear mainly on the parallel and radial components of the RF electric field.
- 2°) Filaments feature very small-scale radial structures in the immediate vicinity of the radiating straps.
- 3°) Filaments decrease in magnitude and change shape when the parallel dielectric constant of the medium is artificially increased in magnitude.
- 4°) Filaments are absent when the antenna box is in vacuum or more generally when it is filled with diagonal dielectric media.
- 5°) Filaments persist even when the confinement magnetic field is fully toroidal. For the sake of simplicity we will study this particular case.

Arguments 1—3 suggest that the filaments consist of highly evanescent Slow Wave electric fields. However a direct excitation of the Slow Wave by the poloidal RF currents imposed on the strap is counter-intuitive, particularly in situation 5. Besides, observation 4 demonstrates a role of the non-diagonal components in the dielectric tensor. These components are traditionally associated with the Fast Mode. Here we propose a simple semi-analytical theory for filament production by an infinitely thin poloidal current strap radiating in toroidally-bounded homogeneous gyrotropic medium with large but finite parallel conductivity. The conditions for exciting the Slow Wave are determined and compared to the phenomenology.

Monochromatic RF electric fields **E** oscillating as $\exp(+\mathrm{i}\omega_0 t)$ ("engineer convention") propagate according to the time-harmonic vectorial equation

$$\nabla\times\nabla\times\mathbf{E}-k_0^2\boldsymbol{\varepsilon}\mathbf{E}=-\mathrm{i}\mu_0\omega_0\mathbf{j}_{\mathbf{ant}} \qquad \text{(A1)}$$

In this equation $k_0=\omega_0/c$ is the wavevector in vacuum, $\mathbf{j}_{\mathbf{ant}}$ is an imposed current source, while the (normalized) dielectric tensor can be found in Eq. (1). When the medium is homogeneous, plane waves oscillating as $\exp(+\mathrm{i}\omega_0 t-\mathrm{i}k_0(n_{//}x+n_\perp z))$ are allowed to propagate. In Fourier space Eq. (A1) becomes (with "engineer conventions")

$$k_0^2\mathbf{K}\hat{\mathbf{E}}=\mathrm{i}\mu_0\omega_0\hat{\mathbf{j}}_{\mathbf{ant}} \quad ; \quad \mathbf{K}=\begin{bmatrix} S-n_{//}^2 & \mathrm{i}D & n_{//}n_\perp \\ -\mathrm{i}D & S-n^2 & 0 \\ n_{//}n_\perp & 0 & P-n_\perp^2 \end{bmatrix}\begin{matrix} y \\ z \\ x \end{matrix} \qquad \text{(A2)}$$

For given parallel refractive index $n_{//}$ the perpendicular refractive indices $n_\perp$ and the electric field polarisations are respectively the solutions of det(**K**)=0 and the associated eigenvectors. In gyrotropic media two modes can exist: the Fast Wave and the Slow Wave. In this appendix we use the simplified dispersion relations valid for large negative P far from the Lower Hybrid resonance S=0. However we retain the full wave polarizations, because they play a key role in filament excitation. The simplified formulas are also valid for any value of P when D=0, i.e. in uniaxial media. The Fast Wave refractive index is given by Eq. (3). The associated (approximate) polarization is ([27], Eq. (22.13), with "engineer convention")

$$E_{yF}\approx-\frac{\mathrm{i}D}{S-n_{//}^2}E_{zF} \quad ; \quad E_{xF}\approx-\frac{n_{\perp F}n_{//}}{P-n_{\perp F}^2}E_{yF}=\frac{\mathrm{i}Dn_{\perp F}n_{//}}{\left(S-n_{//}^2\right)\left(P-n_{\perp F}^2\right)}E_{zF}=P_F\left(n_{\perp F}\right)E_{zF} \qquad \text{(A3)}$$

For large $|P|$, the Fast Wave electric field is nearly transverse to the confinement magnetic field. Yet for finite parallel conductivity and in presence of gyrotropy ($D\neq0$) the Fast Wave carries a small E_x component. The Slow Wave refractive index is given by Eq. (2) .The associated (approximate) polarization is ([27], Eq. (22.14))

$$E_{yS}=-\frac{n_{\perp S}n_{//}}{S-n_{//}^2}E_{xS} \quad ; \quad E_{zS}\approx-\frac{\mathrm{i}D}{n_{\perp S}^2}E_{yS}\approx\frac{\mathrm{i}Dn_{//}}{n_{\perp S}\left(S-n_{//}^2\right)}E_{xS}=P_S^{-1}\left(n_{\perp S}\right)E_{xS} \qquad \text{(A4)}$$

The radiated Slow Wave electric field is nearly transverse to the ignorable direction z. Yet for finite parallel conductivity and in presence of gyrotropy the Slow Wave carries a small E_z component. For $n_{//}^2>>|S|$, the first equation

of (A4) reduces to Eq. (6). We now investigate wave excitation by an infinitely thin poloidal current sheet located in y=0, i.e. in Eq. (A1) we impose

$$\mathbf{j_{ant}}(x,y,z) = j_{zant}(n_{//})\delta(y)\exp(\mathrm{i}\omega_0 t - \mathrm{i}k_0 n_{//} x)\mathbf{e_z} \qquad \text{(A5)}$$

For the sake of simplicity we assume radiating boundary conditions both towards large positive y and large negative y. To incorporate a metallic wall at the back of the antenna box, one can use *a posteriori* the method of images. Under radiating conditions, the poloidal and parallel RF electric fields take the simple form:

$$E_z(n_{//}, y) = E_{zF}(n_{//})\exp(-\mathrm{i}k_0 n_{\perp F}|y|) + E_{zS}(n_{//})\exp(-\mathrm{i}k_0 n_{\perp S}|y|) \qquad \text{(A6)}$$

$$E_x(n_{//}, y) = \mathrm{sgn}(y)\left[P_F(+n_{\perp F})E_{zF}(n_{//})\exp(-\mathrm{i}k_0 n_{\perp F}|y|) + P_S(+n_{\perp S})E_{zS}(n_{//})\exp(-\mathrm{i}k_0 n_{\perp S}|y|)\right] \qquad \text{(A7)}$$

In these expressions either Re($n_\perp$)>0 (outgoing waves) or Im($n_\perp$)<0 (evanescent waves). In expression (A7) sgn(y) appears since both $P_F(n_{\perp F})$ and $P_S(n_{\perp S})$ change signs when $n_\perp$ is reversed (see Eqs. (A3) and (A4)). At the current sheet, we enforce the continuity of the parallel RF electric field as well as

$$(\partial_y E_z)_{y=0^+} - (\partial_y E_z)_{y=0^-} = \mathrm{i}\mu_0\omega_0 j_{zant}(n_{//}) \qquad \text{(A8)}$$

This yields

$$P_F(+n_{\perp F})E_{zF}(n_{//}) + P_S(+n_{\perp S})E_{zS}(n_{//}) = 0 \qquad \text{(A9)}$$

$$n_{\perp F}E_{zF}(n_{//}) + n_{\perp S}E_{zS}(n_{//}) = -\frac{\mu_0 c}{2} j_{zant}(n_{//}) \qquad \text{(A10)}$$

Whence the amplitude of the Slow Wave poloidal RF field.

$$E_{zS}(n_{//}) = \frac{\mu_0 c P_F j_{zant}(n_{//})}{2(n_{\perp F}P_S - n_{\perp S}P_F)} \qquad \text{(A11)}$$

Formula (A11) shows that poloidal RF currents can excite the Slow mode. The qualitative explanation is as follows. Poloidal currents produce RF electric fields oriented in the poloidal direction (Eq. (A8)), i.e. preferentially excite the Fast wave. But the Fast mode can in turn generate a small parallel electric field. To cancel this field at the current sheet it is necessary to produce a Slow Wave component. From Eq. (A9) $E_{zS}(n_{//})$=0 if P_F=0, i.e. for example if D/P=0. In other words the Slow Wave appears only in gyrotropic media with finite parallel conductivity, consistent with observations 3 and 4. Besides $n_{//}\neq 0$ is also required.

Figures 1A.a) – 1.d) illustrate the RF electric fields produced by an infinitely thin current strap radiating in a typical plasma found in **Figure 10** and **Figure 11**. For these conditions all the Fast Wave modes and the Slow Wave modes of the box are evanescent, but the Slow Wave disappears over a smaller radial distance. In these conditions the radial RF field is in phase with the RF current, while the poloidal and parallel RF fields are in phase quadrature. Small-scale features, of millimetric radial extension, appear mainly in the map radial electric field, but are hardly visible for the poloidal electric field, consistent with observations 1 and 2. Across the strap, the parallel electric field swaps signs. This change is continuous but occurs over a small radial width of the same order as for the radial field. Although their spatial structures are different, the ratio of typical amplitudes for the radial and parallel electric fields is consistent with Eq. (6). Since the Fast and Slow waves can be explicitly separated in our model, we verify that the small-scale features are associated with the Slow mode. This is illustrated on **figure 1A**.b) for the parallel electric field. Away from the strap, only the Fast Wave components of the RF fields persist.

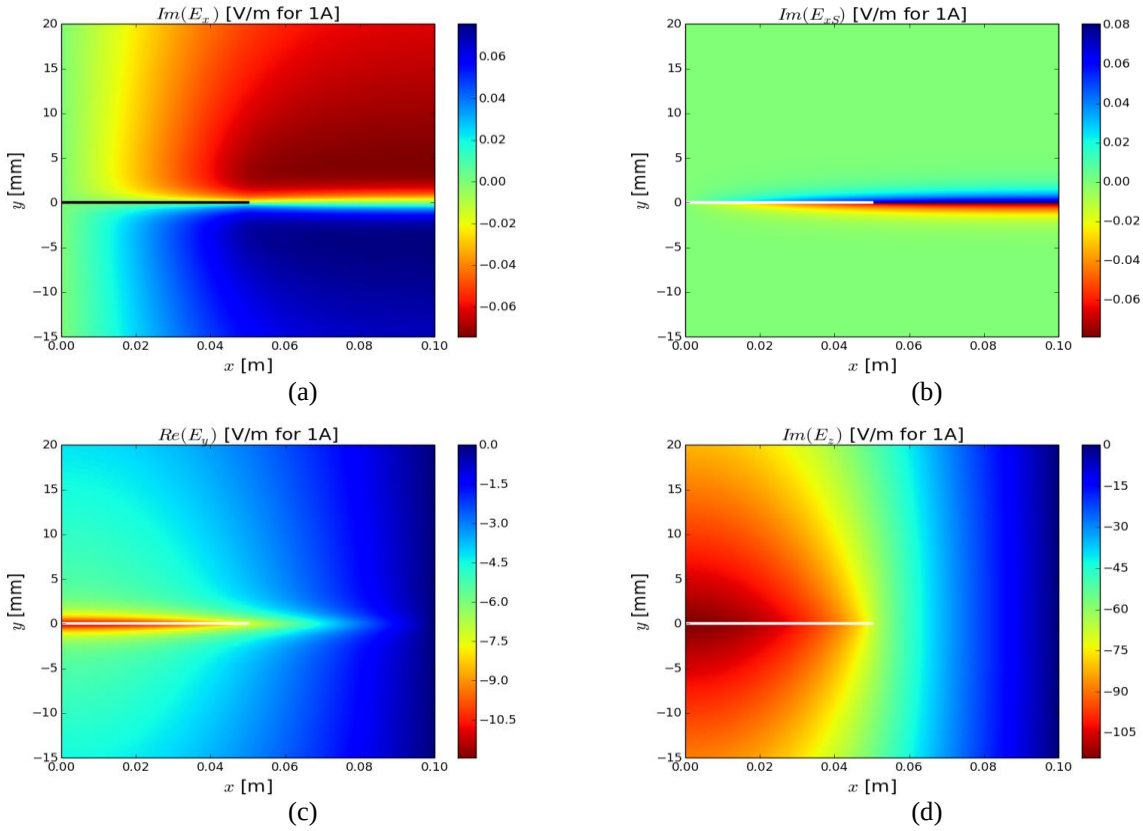

Figures 1A. 2D (toroidal/radial) maps of RF electric fields produced by an infinitely thin current strap of parallel extension $l_{//}$=0.1m. The grid size used here is 2.5×10-5m in y direction and 1.22×10-5m in x direction. The strap is fed with 1A of current distributed regularly over the strap width. The strap is enclosed in a metallic box of parallel extent $L_{//}$=0.2m, with a metallic wall at y=-155mm. The box is filled with homogeneous plasma of dielectric constants P=-15290.0, S=-3.7870, D=13.17. a) Imaginary part of parallel RF electric field, b) idem, slow wave contribution, c) Real part of radial RF electric field, d) Imaginary part of poloidal electric field. Thick horizontal lines : sketch of strap. Only half of the box is represented. Toroidal symmetry relations: $E_x(-x,y)=-E_x(x,y)$; $E_y(-x,y)=+E_y(x,y)$; $E_z(-x,y)=+E_z(x,y)$.

We also tested the evolution of field structures when the parallel dielectric constant is divided by ten. The poloidal electric field is hardly modified, consistent with the expected properties of the Fast Wave. The parallel electric fields increase in magnitude as ~$|P|$, while the amplitude small-scale radial fields scales as ~$|P|^{1/2}$. The shape of the parallel electric field pattern hardly evolves, except close to the strap. The filamentary structures become wider radially, by an approximate factor $|P|^{1/2}$.

Going beyond the qualitative observations 1—5 is challenging, because the spatial pattern of Slow Wave fields likely depends on the detailed spatial distribution of strap RF currents. In our simple 2D model the strap is reduced to an imposed current sheet homogeneous in the ignorable direction. In more refined 3D models the strap is thick, the distribution of RF currents should depend on the poloidal coordinate and should be determined self-consistently.

REFERENCE

1. J. Hillairet, P. Mollard, Y. Zhao, J.-M. Bernard, **B45**, 21st RF conference proceeding, April, 2015 (to be published)
2. R. A. Cairns, Radio-frequency heating of plasmas, Adam Hilger, 1991
3. T.H.Stix, waves in plasmas, AIP Press (1992)
4. J. Jacquot, D. Milanesio, L. Colas, Y. Corre, M. Goniche, J. Gunn, S. Heuraux, M. Kubic and R. Maggiora, Phys. Plasma **21**, 061509 (2014)
5. V. Lancellotti, D. Milanesio, R. Maggiora, G. Vecchi and V. Kyrytsya, Nucl. Fusion **46**(2006) S476-S499
6. A. Messiaen, R. Koch, R.R. Weynants, P. Dumortier, F. Louche, R. Maggiora and D. Milanesio, Nucl. Fusion **50** 025026 (2010)
7. S. Pécoul, S. Heuraux, R. Koch and G. Leclert, Comput. Phys. Commun. **146** 166
8. R. Bilato, M. Brambilla, D. A. Hartmann and A. Parisot, Nucl. Fusion **45** L5-L7 (2005)
9. A. Messiaen and R. Weynants, PPCF, **53** (2011) 085020
10. F. Clairet, L. Colas, S. Heuraux and G. Lombard, PPCF, **46** 1567-1580 (2004)
11. M. J. Mayberry, S.C. Chiu, R.I. Pinsker, R. Prater, Nucl. Fusion 30 N4 pp. 579-597, April 1990
12. P. M. Bellan, Phys. Plasma **1**(11), Nov. 1994
13. S. Puri and M. Tutter, Nucl. Fusion, **13**(1), 1973
14. K. Crombé and D. Van Eester, P1.039, 41th EPS conference on plasma physics, 2014. http://ocs.ciemat.es/EPS2014PAP/pdf/P1.039.pdf
15. J. Jacquot, L. Colas, F. Clairet, M. Goniche, S. Heuraux, J. Hillairet, G. Lombard and D. Milanesio, PPCF **55** 115004 (2013)
16. L. Lu, L. Colas, Numerical tests of wave coupling code , Private communication (2013)
17. http://www.comsol.com/
18. https://www.cst.com/Products/CSTMWS
19. F. Louche, J. Jacquot, K. Crombé, D.Van Eester, **B38**, 21st RF conference proceeding, April, 2015 (to be published)
20. D. Van Eester, K. Crombé, L.F. Lu, **A54**, 21st RF conference proceeding, April, 2015 (to be published)
21. L. Lu, L. Colas, Developing Self consistent Sheath and Waves for ICH-full wave code, Private communication (2014)
22. D. A. D'Ippolito, J .R. Myra, E. F. Jaeger and L. A. Berry, Phys. Plas, **15**, 102501(2008)
23. J. Jacquot, V. Bobkov, L. Colas, S. Heuraux, A. Kˇrivská, L. Lu and J.-M. Noterdaeme, A41, 21st RF conference proceeding, April, 2015 (to be published)
24. K. Crombé, D.Van Eester, R. Koch and V. Kyrytsya, AIP conf. proc. 1580, 318-321 (2014)
25. J. R. Myra and D A D'Ippolito, PPCF **52** 015003 (2010)
26. H. Kohno, J.R. Myra and D.A. D'Ippolito, Phys. Plasma **22**, 072504 (2015)
27. M. Brambilla, Kinetic theory of plasma waves homogeneous plasmas, 1998, Oxford
28. D. Van Eester, K. Crombé and V. Kyrytsya, PPCF, **55** 025002 (2013)
29. D. Milanesio and R. Maggiora, PPCF, 55 045010 (2013)